Editors' Suggestion | Featured in Physics

Broadband Waveguide Cloak for Water Waves

Siyuan Zou,[1,2] Yadong Xu,[3] Razafizana Zatianina,[1] Chunyang Li,[1] Xu Liang,[4] Lili Zhu,[1] Yongqiang Zhang,[1] Guohua Liu,[1] Qing Huo Liu,[5] Huanyang Chen,[2,*] and Zhenyu Wang[1,†]

[1]*College of Civil Engineering and Architecture, Zhejiang University, Hangzhou 310058, China*

[2]*Institute of Electromagnetics and Acoustics and Key Laboratory of Electromagnetic Wave Science and Detection Technology, Xiamen University, Xiamen 361005, China*

[3]*School of Physical Science and Technology and Jiangsu Key Laboratory of Thin Films, Soochow University, Suzhou 215006, China*

[4]*Ocean College, Zhejiang University, Zhoushan 316021, China*

[5]*Department of Electrical and Computer Engineering, Duke University, Durham, North Carolina 27708, USA*

(Received 7 March 2019; published 13 August 2019)

Inspired by electromagnetic waveguide cloaks with gradient index metamaterials, we fabricated a broadband cloak with simply a gradient depth profile on the bottom and without any other structures on the top to confine water waves in a certain area for cloaking regions. The new physics of mode conversion for water waves is first found. The experimental and numerical simulation results are in good agreement and show that the presented device has a nice performance for various situations and is feasible over a broadband of working frequencies. Being easy to construct, this design is potentially of significance for port applications.

DOI: 10.1103/PhysRevLett.123.074501

Introduction.—Oceans are important places for human activities including offshore drilling, offshore wind power, aquaculture, etc. As these activities are subject to the harsh marine environment [1–10], research topics such as how to control water wave propagation at will and to reduce water wave actions play a key role in the wave motion community [11–17]. Conventional methods such as salt marshes [14] and breakwaters [7] have been demonstrated, but only for the purpose of dissipating or attenuating the wave energy.

The past decade has witnessed the development of electromagnetic (EM) metamaterials that have opened up a wide range of opportunities for manipulating the flow of EM waves or light in an unprecedented way [18,19]. Metamaterials are artificial materials comprised of subwavelength engineered blocks (or artificial atoms). With them, numerous amazing phenomena and optical devices have been proposed in theory and well demonstrated in experiments, such as negative refraction [20–22], superlens [23], etc. In particular, with the advent of transformation optics (TO) [24,25], metamaterials exercise significant influence on designing novel optical devices [26]. The most striking example is the invisibility cloak [27–29], which is able to make the light propagating around an obstacle of arbitrary shape or size without any scatterings, as if disappeared. This concept of invisibility cloak is surely tempting in water wave, which may enable some important applications to protect offshore facilities from water wave damages. In fact, because of the similar wave dynamic characteristics, the metamaterial concept can also be extended to other subjects, such as elastic waves [30,31], acoustic waves [32–35], as well as water waves of interest here [11–13,15]. However, the invisibility cloaks based on TO cannot be applied directly to water waves for the required structures are extremely complex and nearly impossible to implement for a perfect one for a broadband of frequencies [11]. Therefore, finding a simple, perfect, and broadband structure is the turning point.

Recently, planar gradient metamaterials [36] have been proposed and well known by their exceptional abilities for controlling light flow and enabling physical phenomena that differ from those observed in their 3D counterparts (i.e., metamaterials). In particular, by integrating the gradient index metamaterials (GIMs) into waveguide systems, the dynamic characteristics of a guided mode can be effectively tailored, based on the mode evolutions. Such a feature leads to devices including mode conversion [36] and asymmetric transmission [37]. It was demonstrated that one can design a waveguide cloak based on mode conversion, by which the propagating modes can be converted into waveguide trapped modes. In this way, one can have a cloak region. Notably, such waveguide cloaks can work in a broadband of frequencies without limitation of polarization, and are easy to fabricate with any complex structures, thus providing a new approach to manipulate the wave.

Inspired by these new approaches, in this work, we design theoretically and demonstrate experimentally a waveguide cloak for water waves by using GIMs. The required GIMs are obtained by only controlling gradient water depth at different positions [38–40]. Both theoretical and experimental results confirm that the designed devices have good cloak performance for a broadband of working frequencies. This work is important in two aspects. For the

 © 2019 American Physical Society

physics aspect, it is demonstrated that only a gradient depth profile on the bottom can help to induce broadband confinements of water waves, thereby with cloaking phenomena. It would be possible to confine water waves with structures on the top, such as the field concentrators [15]. We find here that the mechanism of waveguide mode conversion is also valid for water waves, which make the design much simpler. For the engineering aspect, the cloak is verified to be able to work in a large water tank; hence it should be possible to lead to real port applications.

Construction of a waveguide cloak for water waves.—Based on mode conversion of electromagnetic (EM) waves in Ref. [41], here a waveguide cloak for water waves with a broadband of working frequencies is designed in a parallel-plate waveguide. Such a parallel-plated waveguide can be regarded as the harbor channels in practice. Figure 1(a) shows the schematic plot of the proposed broadband cloak device, a 1D parallel-plate waveguide with two identical GIMs attached to its boundaries (the two black horizontal lines) that mimic the perfect electric conductor (PEC) walls in EM fields. Each GIM, as shown in Fig. 1(b), contains three regions that consist of two symmetric curved-shape parts and one flat-shape part. The GIMs are designed based on the gradient depth profiles for reducing the scattering [38,39].The flat-shape region is composed of a cuboid with the length of L_2 and the height of d. The background water depth is h; thus the water depth over the flat-shape region is a constant value. In the curved-shape regions, the length is L_1 and the height varies from 0 to d gradually, resulting to a position-dependent water depth $h(x)$ changing from the maximal value h to the minimal value h-d, hence with an effective gradient index profile for water waves.

Following the concept of the broadband cloak for EM waves, the water waves propagating through the GIMs regions undergo an effective refractive index profile $n(x)$ that alters gradually due to the changing water depth $h(x)$ [38–40]. As we take a shallow water case, for instance, the water wave has the following nondispersive relationship,

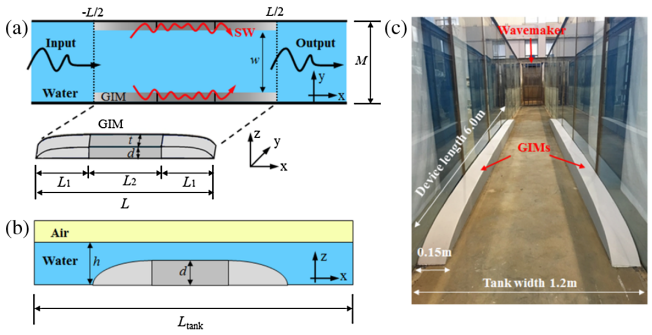

FIG. 1. The concept of a broadband cloak for water waves: (a) The schematic plot of the top view of the cloak device and three-dimensional sketch of GIMs. (b) The side view of the waveguide cloak with GIMs. (c) The experimental photographs of the real cloak device with two GIMs in the water tank.

$$\omega = \sqrt{gh}k, \tag{1}$$

where ω, g, and k are the angular frequency, the acceleration of gravity, and the wave number, respectively. In the background region ($|x| \geq L/2$) of the maximum water depth, the refractive index is 1, while in the flat-shape region ($|x| \leq L_2/2$) of the shallowest water depth, the refractive index is $N_1 = \sqrt{h/(h-d)}$.

The refractive index profile in the curve-shape regions is

$$n(x) = \sqrt{\frac{h}{h-d(x)}}, \qquad (L_2/2 \leq |x| \leq L/2). \tag{2}$$

Finally, Eqs. (3) and (4) can be acquired (See Supplemental Material I for detailed formula derivation [42]),

$$n^2(x) = \frac{2x(N_1^2-1)+L_2-LN_1^2}{L_2-L}, \qquad (L_2/2 \leq |x| \leq L/2), \tag{3}$$

$$d(x) = \frac{h(2x-L)(N_1^2-1)}{2x(N_1^2-1)+(L_2-LN_1^2)}, \qquad (L_2/2 \leq |x| \leq L/2). \tag{4}$$

It is noticed that the relationship between frequency and wave number is usually dispersive, and the maximum effective refractive index in the middle part of the GIMs is small and the wave confinement is thereby not strong enough for the cloaking design. Currently we need to implement a large one to reduce this effect. In addition, the nondispersive approximation of Eq. (1) will ease our design on the required depth profiles (for a dispersive one, the profiles cannot be obtained analytically). Figure 1(c) shows the real cloak device and experimental setup, where the 1D parallel-plate waveguide is a water tank with 60 m × 1.2 m × 2 m (length × width × height), and the GIMs are made of iron sheets which are painted to the walls to prevent oxidization. In experiments, the water is injected into such a tank, with its depth h varying from 0.15 to 0.18 m for various explorations. In addition, a wave maker acting as a wave source is installed at one side of the water tank, which can generate water waves with various amplitudes and the frequency varies from 0.2 to 2 Hz. A wave dissipating device is arranged at the other end of the tank.

For the GIMs, their length and thickness are $L = 6$ m and $t = 0.15$ m, respectively, which means the distance between the two GIMs is $w = 0.9$ m. Usually, these slender structures in the tank will influence the gross flow over the whole width. Nevertheless, the waves we generate here are with small flow and amplitude. In addition, the whole width is about 8 times of the thickness of each GIM, which reduces this effect substantially. The length of the

flat-shape region is $L_2 = 2.44$ m and the height $d = 0.133$ m. In the curved-shape regions, the length is $L_1 = 1.78$ m and the height varies from 0 to $d = 0.133$ m. Given the water depth of h, the shape of the curved-shape regions is given by Eq. (4).

Numerical and experimental water wave analysis.—First, several numerical calculations are carried out to check the cloaking performance of the designed device based on the finite element method. The water waves are incident from the left, as seen in Fig. 1(a). For demonstrating the broadband response and the flexible feature of choosing refractive index, in simulations the working frequency and water depth are considered to be $f =$ 0.6–0.9 Hz and $h = 0.15$–0.18 m. We set all parameters in the simulations, such as the size of the GIMs, the wave tank, the initial water depth h, and the refractive index n on the commercial solver. The walls of the wave tank are hard boundaries and the two ends of the waveguide are perfectly matched layer absorbing boundaries. We used the PDE interface of COMSOL MULTIPHYSICS for simulating the wave patterns by solving the equation $\nabla \cdot (h\nabla\eta) + (\omega^2/g)\eta = 0$. Figures 2(a) and 2(b) illustrate the corresponding numerically simulated field patterns of water waves, which clearly show the mode evolution process of the water waves. For example, as shown in Fig. 2(b), as the incident plane wave (PW) propagates from the left and goes through the region of $x = -L/2$ to $-L_2/2$, it will be converted gradually into two waveguide trapped waves (WTWs) confined in the GIM regions, where the water depth decreases slowly from maximum to minimum. Note that a raised rectangular profile and submerged rectangular plates also support these modes, which are also called "trapped waves" [43]. However, such designs cannot be used to manipulate the modes. In the current version, a continual profile is required for mode conversion and cloaking effect. Earlier works with different models for approximating water wave motion, e.g., mild-slope equations, are recommended as well [44,45]. Note that we do not need any structure on the top to achieve this wave confinement like original work in Ref. [15]. At the flat-shape region from $x = -L_2/2$ to $x = L_2/2$, the WTWs remain unchanged and pass through it. After the position $x = L_2/2$, the WTWs are converted gradually back into PWs with the wave front as perfect as that of incidence, thanks to the symmetric GIM structures. Therefore, the PWs-WTWs-PWs conversion is found for surface water waves. Because of the evanescent features of the WTWs in the flat-shape region, one can find a specific region in the middle of the tank where the amplitudes of the water waves are very small. A sizable object placed in the specific region in the middle of the tank, called the cloak region, has almost no movement as the water waves traveling in the GIM regions. Such a water wave manipulation (confinement and cloaking) has not been reported before. Note that the sizes of the cloak regions in these two cases of Fig. 2 are different, which are dependent on parameters including the size of the waveguide, the size of GIMs, the working frequencies, and the value of N_1. Thus one can further optimize our proposal to obtain a maximized cloak region.

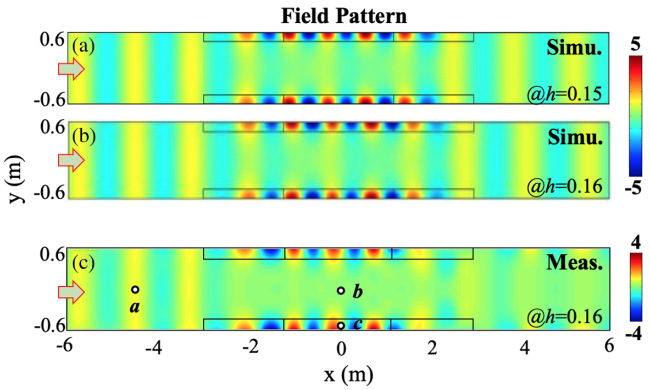

FIG. 2. Field patterns of water waves: (a) The numerically simulated results for $f = 0.7$ Hz and $h = 0.15$ m. (b) The numerically simulated results for $f = 0.7$ Hz and $h = 0.16$ m. (c) The measured results at the condition of $f = 0.7$ Hz and $h = 0.16$ m.

In order to verify the actual stealth characteristics of the waveguide structure, we carried out the water wave experiment at various frequencies and water amplitudes. Wave amplitudes are measured by placing water wave sensors at different positions in the tank. Wave field diagrams are generated from the measured data of the wave amplitudes (See Supplemental Material II for detailed test method [42]). Figure 2(c) shows the experimental results for the case of $f = 0.7$ Hz and $h = 0.16$ m, which are consistent with the simulation results in Fig. 2(b). In fact, kh, the wave steepness (kA), and the Ursell number in the background region are 0.83, 0.0017, and 0.7, respectively. While kh, the wave steepness (kA), and the Ursell number in the GIM parts are 0.17, 0.0046, and 233, respectively. Hence, the background region is approximately in the linear domain of the water wave. While for the GIM parts, the nonlinear effect and viscosity should be carefully considered. Currently, because of the cumulative effect of nonlinearity and viscosity, there is some tiny wavelength mismatching in these two patterns of Figs. 2(b) and 2(c). We solve the model analytically to design the raised beds along the waveguide walls. This design is a kind of inverse problem with difficulty, and the simplified model is operational based on Eq. (1). Some sophisticated numerical methods are necessary to improve the simulation and optimize the design of GIMs in the future. The mode evolution process of PWs-WTWs-PWs conversion can also be seen clearly. While the transmission of output water wave is less than unity, which results from the loss of water wave, especially the viscosity in the GIM parts. In particular, in the middle ($-L_2/2 < x < L_2/2$) most of water waves are confined in GIM regions with field amplitudes much larger than that of incidence, and one can see a cloak region with a weak field distribution compared to that of incidence. The related

dynamic wave patterns can also be visualized in videos in the Supplemental Material II [42]. We can reduce the length of the raised sections to reduce the effect of viscous losses, yet the cloaking area is also reduced.

To further analyze the invisibility characteristics of the waveguide cloak, we quantize the wave amplitudes at three different positions that are denoted by points a, b, and c in Fig. 2. a is in the incident wave region, b is in the cloak region, and c is in the GIM region. Figures 3(a) and 3(b) illustrate both the measured and simulated results of amplitude ratios of point b and point c vs the working frequency for $h = 0.15$ m and $h = 0.16$ m, respectively. Here the amplitude ratios are $\beta_b = A_b/A_a$ and $\beta_c = A_c/A_a$, where A_a, A_b, and A_c are the corresponding amplitudes at points a, b, and c, respectively. A_a is about 1 mm. Both the measured and simulated results are neatly consistent. The results in Figs. 3(a) and 3(b) clearly show that the designed cloak makes the amplitudes at point b decrease greatly and that at point c increase a lot, for the working frequency from 0.6 to 0.9 Hz, which demonstrates a broadband response. Furthermore, we examine the influence of different water depths on the cloaking performance. Figure 3(c) plots the results of the amplitude ratio vs water depth at a fixed frequency of $f = 0.7$ Hz and A_a about 1.2 mm, where both the simulated and experimental results also coincide very well. As h varies from 0.15 to 0.18 m, the amplitude ratio is still quite tiny for point b. However, the cloaking effect is compromised a bit. While for point c, it is enhanced as well, yet the ratio drops for a deeper water depth. This is because the deeper water depth is related to a smaller refractive index profile, hence with a smaller cloaking region.

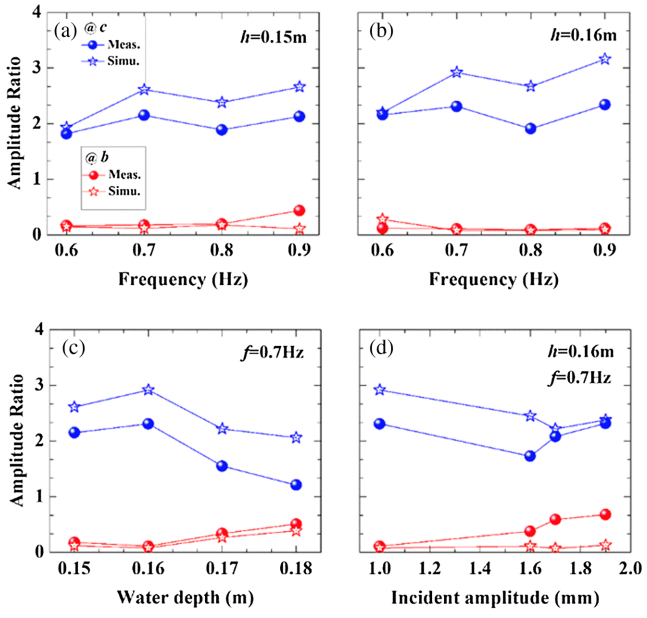

FIG. 3. Comparison between the experimental results and simulation results for various working frequencies, water depths, and incident amplitude: (a) working frequency response for $h = 0.15$ m and $A_a = 1$ mm; (b) working frequency response for $h = 0.16$ m and $A_a = 1$ mm; (c) water depth influence for $f = 0.7$ Hz and $A_a = 1.2$ mm; (d) incident amplitude influence for $h = 0.16$ m and $f = 0.7$ Hz.

In addition, from the simulations, the incident amplitude of the wave does not affect the cloaking performance, but in practice, it is not the case because the nonlinearity should be considered. Figure 3(d) shows the corresponding results for $f = 0.7$ Hz and $h = 0.16$ m. One can see that as the incident amplitude A_a increases, the numerical results are almost tiny constants at point b, but the measured results increase slowly, making the cloak performance degrade, which should be further optimized in the future with the nonlinearity to be considered in theory. Nevertheless, from the above analysis, the current cloak works well for quite a broadband of frequencies, and for various water depths and incident amplitudes of the waves (as long as they are not too big to avoid nonlinearity). The device could be very useful, especially at point c, where it could be used to collect wave energy, as we have also done in the concentrator experiments [15], while at point b, it could be used to calm the water waves in ports.

Potential application.—The design of this waveguide can also be applied in practice, such as offshore wharves or ports. Near the coast, we often need to build a number of side-by-side wharves. The wharves are open at one side and closed on the other. If we cut the abovementioned waveguide into halves and elongate the flat-shape section to 4.22 m (to show the cloak effect more clearly), by putting the same five components in a row, we obtain the "wharves." The leftmost is an open boundary, and the rightmost is the rigid reflection boundary, and between each component there are also the rigid reflection boundaries. This design is similar to the actual coastal dock. We simulate the wave patterns of different incident waves at $h = 0.16$ m water depth with $f = 0.9$ Hz. Both the field pattern and amplitude are plotted for a plane wave

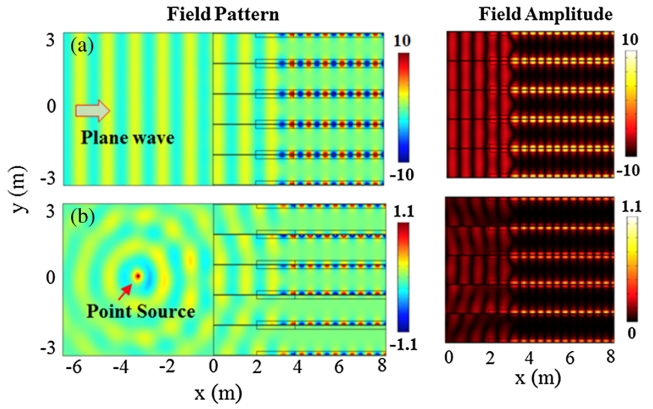

FIG. 4. The simulated field pattern and field amplitude of the designed wharf for the case of $f = 0.9$ Hz and $h = 0.16$ m for (a) a plane wave incidence and (b) a point source.

incidence in Fig. 4(a) and a point source in Fig. 4(b). At the right-hand side, there are five cloaking regions where the waves are almost diminished. Hence, the designed channels are very robust for different incident waves, and will be of important utility.

Conclusions.—Inspired by the concept of waveguide cloaks in EM fields, we design theoretically and demonstrate experimentally a cloak device for water waves, which can be applied to wharves for controlling water waves. The experimental results agree well with numerical simulations and they confirm that the designed device has a desirable cloaking performance for various situations (such as different water depths and incident wave amplitudes) and for a broadband of frequencies. The underlying mechanism is based on mode conversion that the device converts the PWs into WTWs and converts them back to PWs. The new physics found here for water waves eases the cloaking design by simply setting up a gradient depth profile on the bottom without any other structures on the surface. In order to visualize the invisibility effect, we put a small toy boat onto the water surface, as shown in Fig. S7 in Supplemental Material III, where we give the recorded videos of the movement of the boat [42]. Our proposal shows easy, low-cost, and potential applications in ports or wharves to calm the water waves during cargo loading or unloading, etc. Note that there are also other alternative ways to cloak water waves, such as using resonating obstacles in the water-wave channel and so on [45,46]. All of this should be further tested in real world situations. Hence, it is desirable for scientists in engineering and physics to work together for actual practical utility. The reader could also find the effort on sea reduction in harbors and coastal engineering in Ref. [47]. We hope that our work can be verified in real ports or wharves in the near future.

This work was supported by the National Basic Research Programme of China (Grant No. 2013CB035901), the National Natural Science Foundation of China (Grants No. 11874311, No. 11604229, No. 51779224, No. 51579221, No. 51279180, and No. 51079127) and the Fundamental Research Funds for the Central Universities (Grant No. 20720170015).

S. Z., Y. X., R. Z., and C. L. contributed equally to this work. Z. W. and H. C. conceived the idea and supervised the project.

*kenyon@xmu.edu.cn
†wzyu@zju.edu.cn

[1] Z. J. Mark, L. A. Cristiana, and K. Willet, Taming hurricanes with arrays of offshore wind turbines, Nat. Clim. Change **4**, 195 (2014).
[2] V. Roeber and D. J. Bricker, Destructive Tsunami-like wave generated by surf beat over a coral reef during typhoon Haiyan, Nat. Commun. **6**, 7854 (2015).
[3] T. S. Hristov, S. D. Miller, and C. A. Friehe, Dynamical coupling of wind and ocean trough wave-induced air flow, Nature (London) **422**, 55 (2003).
[4] A. Chabchoub, N. Hoffmann, M. Onorato, and N. Akhmediev, Super rogue waves: Observation of higher-order breather in water waves, Phys. Rev X **2**, 011015 (2012).
[5] A. Arns, S. Dangendorf , J. Jensen, S. Talke, J. Bender, and C. Pattiaratchi, Sea-level rise induced amplification of coastal protection design heights, Sci. Rep. **7**, 40171 (2017).
[6] S. C. Daniel, A. Avdis, P. A. Allison, H. D. Johnson, J. Hill, M. D. Piggott, M. H. Amir Hassan, and A. Razak Damit, Tidal dynamics and mangroves carbon sequestration during the Oligo-Miocene in the South China Sea, Nat. Commun. **8**, 15698 (2017).
[7] C. Brysson, Wave action on vertical wall breakwaters, Nature (London) **136**, 283 (1935).
[8] C. M. Duarte, I. J. Losada, I. E. Hendriks, I. Mazarrasa, and N. Marba, The role of coastal plant communities for climate change mitigation and adaptation, Nat. Clim. Change **3**, 961 (2013).
[9] S. Fagherazzi, Coastal processes: Storm-proofing with marshes, Nat. Geosci. **7**, 701 (2014).
[10] A. Chabchoub, N. P. Hoffmann, and N. Akhmediev, Rogue Wave Observation in a Water Tank, Phys. Rev. Lett. **106**, 204502 (2011).
[11] M. Farhat, S. Enoch, S. Guenneau, and A. B. Movchan, Broadband Cylindrical Acoustic Cloak for Linear Surface Waves in a Fluid, Phys. Rev. Lett. **101**, 134501 (2008).
[12] Z. Wang, C. Li, Z. Razafizana, P. Zhang, and Y. Zhang, Carpet cloak for water waves, Phys. Rev. E **96**, 053107 (2017).
[13] C. P. Berraquero, A. Maurel, P. Petitjeans, and V. Pagneux, Experimental realization of a water-wave metamaterial shifter, Phys. Lett. E **88**, 051002 (2013).
[14] M. Iris *et al.*, Wave attenuation over coastal salt marshes under storm surge conditions, Nat. Geosci. **7**, 727 (2014).
[15] C. Li, L. Xu, L. Zhu, S. Zou, Q. Huo Liu, Z. Wang, and H. Chen, Concentrators for Water Waves, Phys. Rev. Lett. **121**, 104501 (2018).
[16] Z. Wang, P. Zhang, X. Nie, and Y. Zhang, Manipulating water wave propagation via gradient index media, Sci. Rep. **5**, 16846 (2015).
[17] Y. Yang, H. Wang, F. Yu, Z. Xu, and H. Chen, A metasurface carpet cloak for electromagnetic, acoustic and water waves, Sci. Rep. **6**, 20219 (2016).
[18] W. Cai and V. Shalaev, *Optical Metamaterials: Fundamentals and Applications* (Springer, New York, 2009).
[19] T. J. Cui, D. R. Smith, and R. Liu, *Metamaterials: Theory, Design and Applications* (Springer, New York, 2010).
[20] J. B. Pendry, Negative Refraction Makes a Perfect Lens, Phys. Rev. Lett. **85**, 3966 (2000).
[21] D. R. Smith, J. B. Pendry, and M. C. K. Wiltshire, Metamaterials and negative refractive index, Science **305**, 788 (2004).
[22] R. A. Shelby, D. R. Smith, and S. Schultz, Experimental verification of a negative index of refraction, Science **292**, 77 (2001).
[23] X. Zhang and Z. Liu, Superlenses to overcome the diffraction limit, Nat. Mater. **7**, 435 (2008).

[24] J. B. Pendry, D. Schurig, and D. R. Smith, Controlling electromagnetic fields, Science **312**, 1780 (2006).
[25] U. Leonhardt, Optical conformal mapping, Science **312**, 1777 (2006).
[26] H. Chen, C. T. Chan, and P. Sheng, Transformation optics and metamaterials, Nat. Mater. **9**, 387 (2010).
[27] D. Schurig, J. J. Mock, B. J. Justice, S. A. Cummer, J. B. Pendry, A. F. Starr, and D. R. Smith, Metamaterial electromagnetic cloak at microwave frequencies, Science **314**, 977 (2006).
[28] D. Shin, Y. Urzhumov, Y. Jung, G. Kang, S. Baek, M. Choi, H. Park, K. Kim, and D. R. Smith, Broadband electromagnetic cloaking with smart metamaterials, Nat. Commun. **3**, 1213 (2012).
[29] H. F. Ma and T. J. Cui, Three-dimensional broadband ground-plane cloak made of metamaterials, Nat. Commun. **1**, 21 (2010).
[30] N. Stenger, M. Wilhelm, and M. Wegner, Experiments on Elastic Cloaking in Thin Plates, Phys. Rev. Lett. **108**, 014301 (2012).
[31] G. Ma, C. Fu, G. Wang, P. del Hougne, J. Christensen, Y. Lai, and P. Sheng, Polarization bandgaps and fluid-like elasticity in fully solid elastic metamaterials, Nat. Commun. **7**, 13536 (2016).
[32] S. A. Cummer, J. Christensen, and A. Alu, Controlling sound with acoustic metamaterials, Nat. Rev. Mater. **1**, 16001 (2016).
[33] C. Z. Shi, D. Marc, Y. Wang, and X. Zhang, High-speed acoustic communication by multiplexing orbital angular momentum, Proc. Natl. Acad. Sci. U.S.A. **114**, 7250 (2017).
[34] Z. Y. Liu *et al.*, Locally resonant sonic materials, Science **289**, 1734 (2000).
[35] B. Assouar, B. Liang, Y. Wu, Y. Li, J.-C. Cheng, and Y. Jing, Acoustic metasurfaces, Nat. Rev. Mater. **3**, 460 (2018).
[36] Y. Xu, Y. Fu, and H. Y. Chen, Planar gradient metamaterials, Nat. Rev. Mater. **1**, 16067 (2016).
[37] Y. Xu, C. Gu, B. Hou, Y. Lai, J. Li, and H. Chen, Broadband waveguiding of light without polarization limitations, Nat. Commun. **4**, 2561 (2013).
[38] F. Bampi and A. Morro, Gravity waves in water of variable depth, Il Nuovo Cimento **1C**, 377 (1978).
[39] F. Bampi and A. Morro, Water wave theories and variational principles, Il Nuovo Cimento **2C**, 352 (1979).
[40] D. G. Provis and R. Radok, *Waves on Water of Variable Depth*, Lecture Notes in Physics (Springer, Berlin, Heidelberg, 2005), Vol. 64.
[41] C. Gu, Y. Xu, S. Li, W. Lu, J. Li, H. Chen, and B. Hou, A broadband polarization-insensitive cloak based on mode conversion, Sci. Rep. **5**, 12106 (2015).
[42] See Supplemental Material at http://link.aps.org/supplemental/10.1103/PhysRevLett.123.074501 which contains three sections: I. Formula derivation, II.test method, and III. experimental videos of a toy boat.
[43] C. M. Linton and D. V. Evans, Trapped modes above a submerged horizontal plater, Q. J. Mech. Appl. Math. **44**, 487 (1991).
[44] R. Porter and D. Porter, Interaction of water waves with three-dimensional periodic topography, J. Fluid Mech. **434**, 301 (2001).
[45] R. Porter, Cloaking in water waves, in *Handbook of Metamaterials and Plasmonics*, Vol. 2: Elastic, Acoustic, and Seismic Metamaterials edited by S. A. Maier (World Scientific Singapore, 2018).
[46] T. Bobinski, A. Maurel, P. Petitjeans, and V. Pagneux, Backscattering reduction for resonating obstacle in water-wave channel, J. Fluid Mech. **845**, R4 (2018).
[47] C. C. Mei, *The Applied Dynamics of Ocean Surface Waves* (Wiley-Interscience, Singapore, 1983).